Magnetospheric Multiscale Observations of Markov Turbulence on Kinetic Scales

Wiesław M. Macek & Dariusz Wójcik

Space Research Centre, Polish Academy of Sciences,

Bartycka 18 A, 00-716 Warsaw, Poland;

e-mail: macek@cbk.waw.pl, http://www.cbk.waw.pl/~macek

https://orcid.org/0000-0002-8190-4620

dwojcik@cbk.waw.pl, https://orcid.org/0000-0002-2658-6068

CBK PAN, 30 November 2023

Plan of Presentation

1. Introduction
   - Importance of Turbulence
   - Research Hypothesis (small kinetic scales)
   - Markov Turbulence on Kinetic scales
2. Data from the *MMS* Mission
   - Magnetic Field Instrument
   - Data Resolutions
3. Methods
   - Chapman-Kolmogorov Condition
   - Kramers-Moyal Expansion
   - Fokker-Planck Equation
4. Observations of Markov Turbulence
   - near the Bow Shock (BS)
   - inside the Magnetosheath (SH)
   - near the Magnetopause (MP)
5. Conclusions

Abstract

We apply Fokker-Planck equation to investigate processes responsible for turbulence in space plasma. In our previous studies, we have shown that turbulence in the inertial range of hydromagnetic scales exhibits Markov properties [Strumik & Macek(2008a), Strumik & Macek(2008b)]. We have extended this statistical approach on much smaller scales, where kinetic theory should be applied. Namely, we have presented the results of the statistical analysis of magnetic field fluctuations in the Earth's magnetosheath based on the *Magnetospheric Multiscale* (*MMS*) mission [Macek et al.(2023)]. Here we compare the characteristics of turbulence behind the bow shock, inside the magnetosheath, and near the magnetopause [Macek & Wójcik(2023)]. We prove that the second order approximation of the Fokker-Planck equation leads to kappa distribution of the probability density function provided that the first Kramers-Moyal coefficient is linear and the second term is quadratic, describing drift and diffusion correspondingly, which is a generalization of the Ornstein-Uhlenbeck process. In this case the power-law distributions are recovered. For some moderate scales we have the kappa distributions described by various peaked shapes with heavy tails. In particular, for large values of the kappa parameter this is reduced to the normal Gaussian distribution. The obtained results on kinetic scales could be important for a better understanding of the physical mechanism governing turbulent systems in laboratory and space.

Keywords: *Kinetic scales, Markov processes,* MMS *probe, Plasmas, Solar wind, Turbulence*

Acknowledgments. This work has been supported by the National Science Centre, Poland (NCN), through grant No. 2021/41/B/ST10/00823.

Importance of Turbulence

Turbulence is a complex phenomenon that notwithstanding progress in magnetohydrodynamic simulations is still a challenge for natural sciences [Frisch(1995)], because physical mechanisms responsible for turbulence cascade are not clear [Biskamp(2003)]. Fortunately, collisionless solar wind plasma can be considered natural laboratories for investigating this complex dynamical system [Bruno & Carbone(2016)].

MMS Observations of Turbulence on Kinetic Scales

- We have confirmed clear breakpoints in the magnetic energy spectra, which occurs near the ion gyrofrequencies behind the bow shock, inside the magnetosheath, and before leaving the magnetosheath.

- We have also observed that the spectrum steepens at these points to power exponents in the kinetic range from -5/2 to -11/2 for the magnetic field data of the highest resolution available within the *MMS* mission.

- Now we present the results of our analysis, where we check whether the solutions of the Fokker-Planck equation are consistent with experimental probability density functions (PDFs).

List of selected *MMS 1* interval samples (hh.min:ss)

Case	Resolution	Time (y.m.d)	Loc.	Begin	End	$\theta_{\mathrm{Bn}}(^\circ)$	M_{A}	β	M_{ms}
(a)	High	2015.12.28	BS	01.48:04	01.52:59	35.8 ± 7	19.3	4.5	8.7
(b)	Low	2015.12.28	SH	06.19:00	09.45:59	46.6 ± 21	19.9	4.9	8.7
(c)	High	2016.12.27	MP	11.30:24	11.32:13	32.0 ± 13	12.8	2.2	7.5

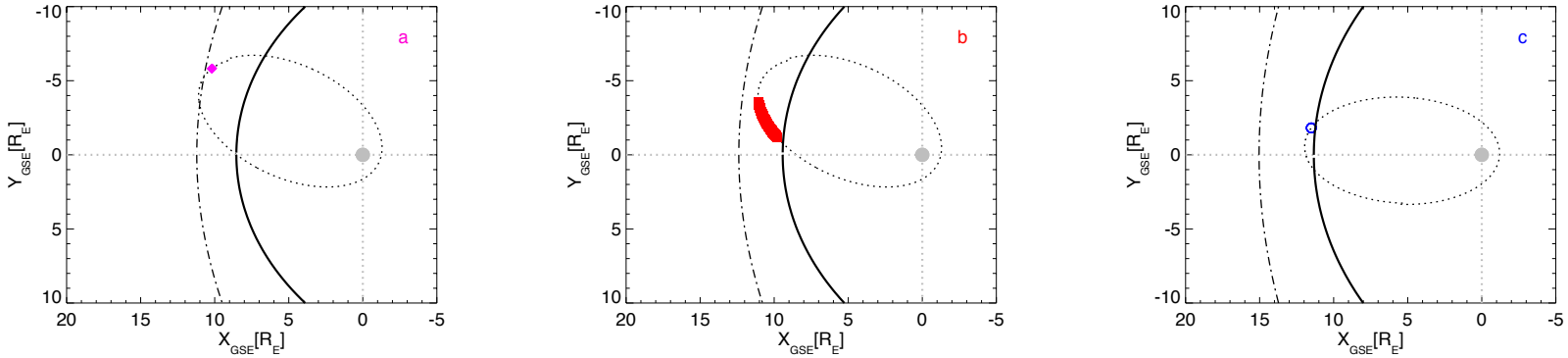

*

MMS 1 spacecraft trajectory in the magnetosheath: (a) behind the bow shock, (b) inside the magnetosheath, and (c) near the magnetopause, from (Macek et al. 2018).

Characteristic plasma parameters values

Parameters	case *(a)* **BS**	case *(b)* **SH**	case *(c)* **MP**
$< B >$ [nT]	18.85	18.23	21.75
f_{ci} [Hz]	0.25	0.24	0.29
f_{ce} [Hz]	528	510	609
T_i [eV]	420	392	574
T_e [eV]	46	43	68
r_{Li} [km]	119	119	120.5
r_{Le} [km]	0.86	0.85	0.9
λ_i [km]	46.65	41	61
λ_e [km]	1.05	0.94	1.35
$f_{\lambda i}$ [Hz]	0.55	0.41	0.45
$f_{\lambda e}$ [Hz]	24.5	18.1	20.1

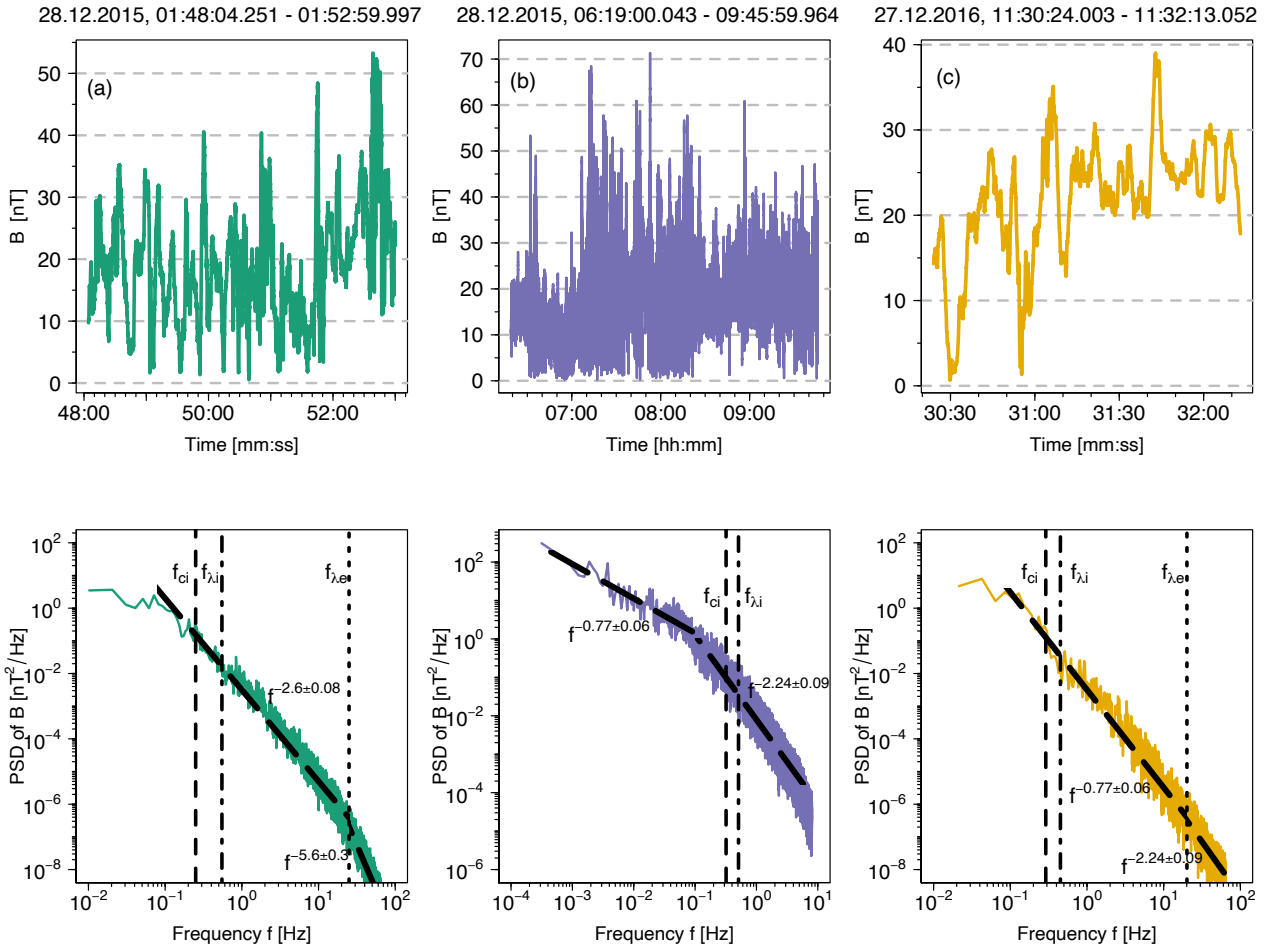

Figure 1: Time series of the magnetic field strength $B = |\mathbf{B}|$ of the *MMS* data with the corresponding spectra in the magnetosheath (a) near the bow shock (BS), (b) inside the magnetosheath (SH), and (c) near the magnetopause (MP) plotted with three different colors. Average ion gyrofrequency (f_{ci}), as well as a characteristic Taylor's shifted frequencies for ions ($f_{\lambda i}$) and electrons ($f_{\lambda e}$) are shown by the dashed, dashed-dotted, and dotted lines, respectively, see Table 1 of Ref. (Macek et al. 2018).

Methods of Data Analysis

We use the increments of a characteristic magnetic field $B = |\mathbf{B}|$ describing a turbulent system at each time t and a given scale τ

$$b_\tau(t) = B(t+\tau) - B(t). \tag{1}$$

We assume that the fluctuations b_τ in a larger scale τ are transferred to smaller and smaller scales. Therefore, turbulence cascade may be regarded as a stochastic process with the N-point joint transition conditional **probability density function** (PDF) $P(b_1,\tau_1|b_2,\tau_2,\ldots,b_N,\tau_N)$ defined by the following conditional probability distribution density functions
$P(b_i,\tau_i|b_j,\tau_j) = P(b_i,\tau_i;b_j,\tau_j)/P(b_j,\tau_j)$,
with the unconditional probability $P(b_j,\tau_j)$.

This process is Markovian if the N-point joint transition conditional probability distribution is 'memoreless' and can therefore be determined by the initial probability density function (PDF) $P(b_1,\tau_1|b_2,\tau_2)$.

Chapman-Kolmogorov Condition is satisfied for Markov turbulence:

$$P(b_1,\tau_1|b_2,\tau_2) = \int_{-\infty}^{+\infty} P(b_1,\tau_1|b',\tau')P(b',\tau'|b_2,\tau_2)db', \tag{2}$$

where $\tau_1 < \tau' < \tau_2$. We use

Kramers-Moyal Expansion

$$-\frac{\partial P(b,\tau|b',\tau')}{\partial\tau} = \sum_{k=1}^{\infty}\left(-\frac{\partial}{\partial b}\right)^k D^{(k)}(b,\tau)P(b,\tau|b',\tau'), \tag{3}$$

where the coefficients $D^{(k)}(b,\tau)$ are given by the moments of the conditional PDFs

$$D^{(k)}(b,\tau) = \frac{1}{k!}\lim_{\tau\to\tau'}\frac{1}{\tau-\tau'}\int_{-\infty}^{+\infty}(b'-b)^k P(b',\tau'|b,\tau)db', \tag{4}$$

in the limit $\tau \to \tau'$.

Fokker-Planck Equation

If the fourth-order coefficient vanishes, then according to the Pawula's theorem, $D^{(k)}(b,\tau) = 0$ for $k \geq 3$, and the series in Equation (3) stops after the second term. Hence the Fokker-Planck equation (3) determining the evolution of the transition probability has the following reduced form [Risken (1996)]:

$$-\frac{\partial P(b,\tau|b',\tau')}{\partial \tau} = \Big[-\frac{\partial}{\partial b}D^{(1)}(b,\tau) + \frac{\partial^2}{\partial b^2}D^{(2)}(b,\tau)\Big]P(b,\tau|b',\tau'), \tag{5}$$

where the first and second terms, are responsible for the drift and diffusion processes, respectively. In this case the following well-known Langevin equation

$$-\frac{\partial b}{\partial \tau} = D^{(1)}(b,\tau) + \sqrt{D^{(2)}(b,\tau)}\Gamma(\tau), \tag{6}$$

for the delta-correlated Gaussian white noise $\langle \Gamma(\tau)\Gamma(\tau')\rangle = 2\delta(\tau - \tau')$, and $\langle \Gamma(\tau)\rangle = 0$ is satisfied [Rinn et al.(2016)].

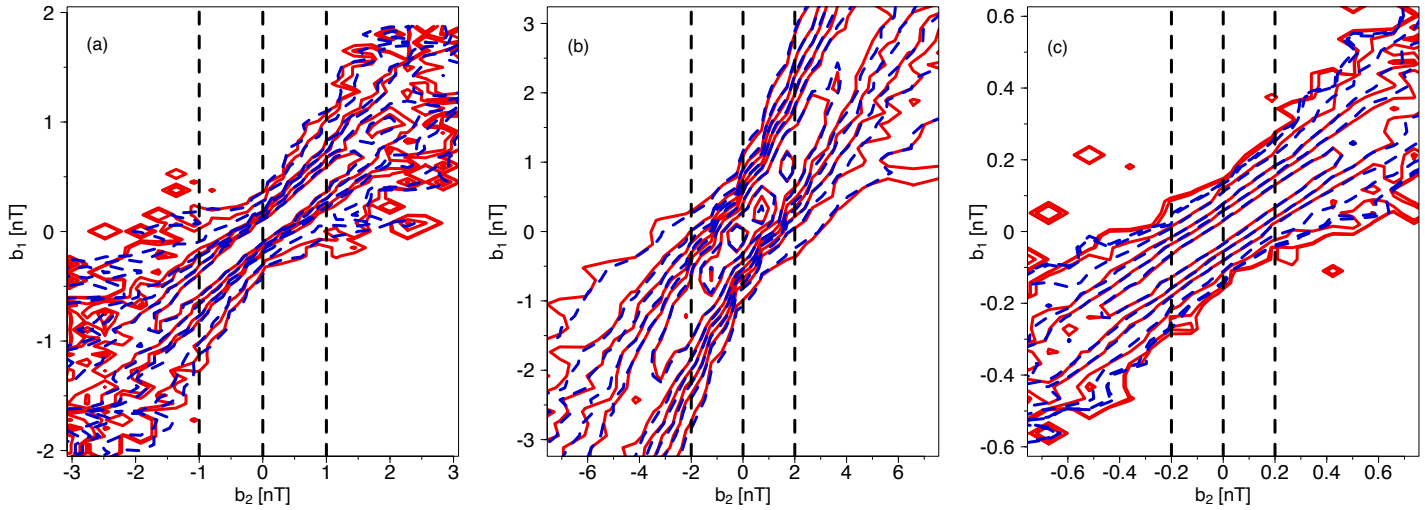

Figure 2: Comparison of the observed contours plots (red solid curves) of conditional probabilities at various scales τ reconstructed from the *MMS* magnetic field strength (a) just behind the bow shock (BS), (b) inside the magnetosheath (SH), and (c) near the magnetopause (MP), corresponding to Figure 1, with those reconstructed (dashed blue curves) according to the Chapman-Kolmogorov condition. The subsequent isolines correspond to the following decreasing levels of the conditional probability density function (PDF), from the middle of the plots, for b_τ: case (a) 2, 1.1, 0.5, 0.3, 0.05, 0.01; case (b) 5, 1, 0.7, 0.45, 0.3, 0.22, 0.15, 0.1, 0.05; case (c) 7, 3.3, 1.3, 0.3, 0.08, 0.06.

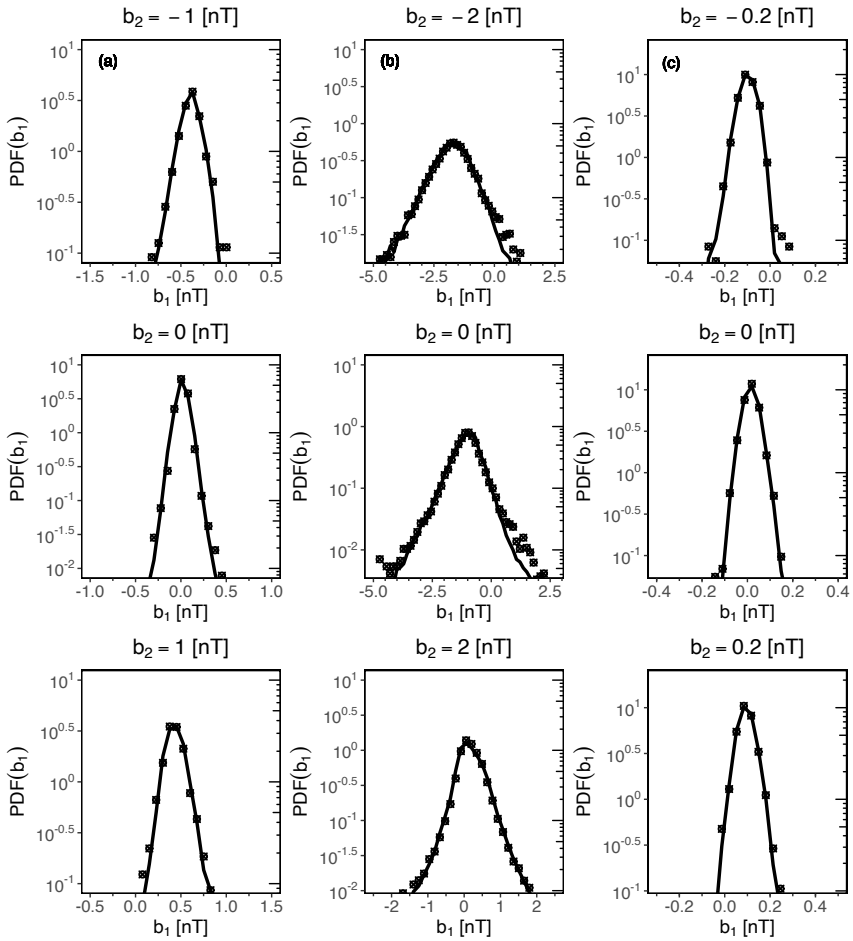

Figure 3: Comparison of cuts through $P(b_1, \tau_1 | b_2, \tau_2)$ for the fixed values of increments b_2: (a) behind the bow shock (BS), (b) inside the magnetosheath (SH), and (c) near the magnetopause (MP), with τ_1 = 0.02 s, τ' = 0.0278 s, and τ_2 = 0.0356 s in cases (a) and (c), and with τ_1 = 0.2 s, τ' = 0.2625 s, and τ_2 = 0.325 s in case (b).

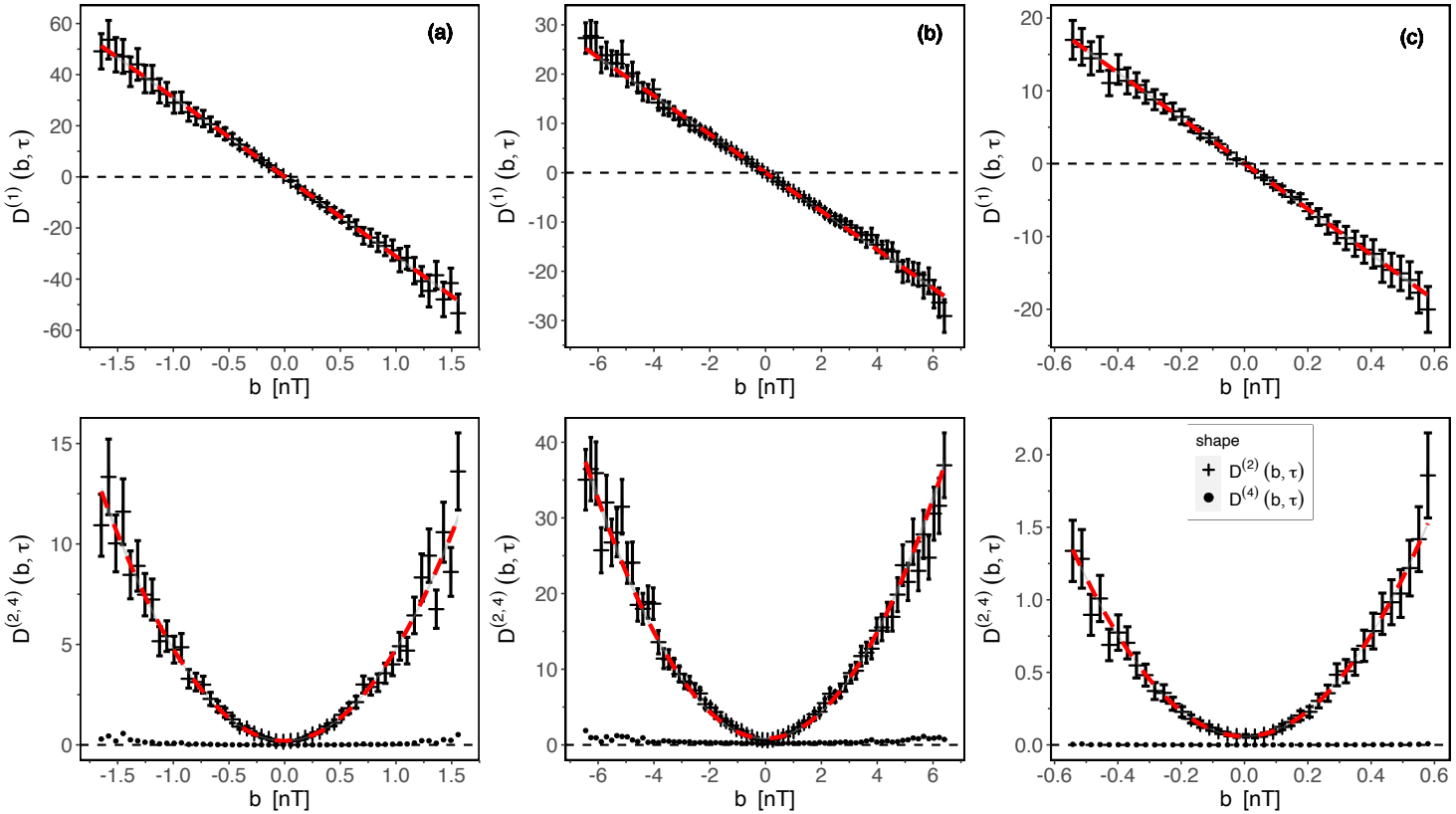

Figure 4: The first and second finite-size Kramers-Moyal coefficients depending on the magnetic field increments b for the strength of the magnetic field $B = |\mathbf{B}|$. The dashed red lines show the best fits to the calculated values of $D^{(1)}(b,\tau)$ and $D^{(2)}(b,\tau)$ with $D^{(4)}(b,\tau)$ = 0, according to the Pawula's theorem.

Kramers-Moyal Coefficients

The best-obtained fits to these lowest-order coefficients are linear

$$D^{(1)}(b,\tau) = -a_1(\tau)b \tag{7}$$

and quadratic functions of b

$$D^{(2)}(b,\tau) = a_2(\tau) + b_2(\tau)b^2, \tag{8}$$

respectively, where the appropriate fitted parameters a_k for k = 1 and 2 and b_2 depend on the time scale τ.
This corresponds to the generalized Ornstein-Uhlenbeck process.

For a usual Ornstein-Uhlenbeck process, we have

$$\begin{cases} D^{(1)}(b,\tau) = -a_1(\tau)b = \gamma b, \\ D^{(2)}(b,\tau) = a_2(\tau) = D = \text{const.} \end{cases} \tag{9}$$

The equation for the transition probability

$$\frac{\partial P(b,\tau|b',\tau')}{\partial \tau} = \gamma \frac{\partial}{\partial b}[b\,P(b,\tau|b',\tau')] + D\frac{\partial^2}{\partial b^2}P(b,\tau|b',\tau'), \tag{10}$$

with the solution of the Gaussian distribution ($\tau > \tau'$) for $\gamma > 0$

$$P(b,\tau|b',\tau') = \sqrt{\frac{\gamma}{2\pi D(1-e^{-2\gamma(\tau-\tau')})}}\exp\Big[-\frac{\gamma(b-e^{-\gamma(\tau-\tau')}b')^2}{2D(1-e^{-2\gamma(\tau-\tau')})}\Big]. \tag{11}$$

The stationary solutiun is recovered for $\gamma(\tau-\tau') \gg 1$

$$P_s(b) = \sqrt{\frac{\gamma}{2\pi D}}\exp\Big(-\frac{\gamma b^2}{2D}\Big). \tag{12}$$

In the limit $\gamma \to 0$ we have the Wiener process.

Wiener Process

In particular,

$$\begin{cases} D^{(1)}(b,\tau) = 0, \\ D^{(2)}(b,\tau) = D = \text{const.} \end{cases} \tag{13}$$

The diffusion equation

$$\frac{\partial P(b,\tau|b',\tau')}{\partial \tau} = D\frac{\partial^2}{\partial b^2}P(b,\tau|b',\tau'), \tag{14}$$

with the initial conditions $P(b,\tau|b',\tau') = \delta(b-b')$ the solution reads

$$P(b,\tau|b',\tau') = \frac{1}{\sqrt{4\pi D(\tau-\tau')}}\exp\Big(-\frac{(b-b')^2}{4D(\tau-\tau')}\Big). \tag{15}$$

The general solution with the initial distribution $P(b',\tau')$ is $P(b,\tau) = \int_{-\infty}^{+\infty} P(b,\tau|b',\tau')P(b',\tau')db'$ the Green function of Equation (14.

Moreover, it appears that all of these parameters exhibit a power-law dependence on temporal scale τ:

$$\begin{cases} a_1(\tau) = A\tau^{\alpha}; \\ a_2(\tau) = B\tau^{\beta}; \\ b_2(\tau) = C\tau^{\gamma}, \end{cases} \tag{16}$$

where the values for all of the logarithmized parameters $A, B, C \in \mathbb{R}$, as well as the $\alpha, \beta, \gamma \in \mathbb{R}$ are given in Table 2.

Table 2: Fitted parameters for power-law dependence of first- and second-order Kramers—Moyal coefficients of Eqs. (7), (8), and (16) as functions of scale τ

Case	$\log_{10}(A)$	α	$\log_{10}(B)$	β	$\log_{10}(C)$	γ
(a)	0.6989 ± 0.0225	-1.1191 ± 0.0089	-0.4946 ± 0.1259	1.1631 ± 0.0498	0.5854 ± 0.0706	-1.7325 ± 0.0279
(b)	0.1837 ± 0.0139	-1.0417 ± 0.0100	-0.4666 ± 0.0160	0.5425 ± 0.0116	0.4183 ± 0.0163	-1.2233 ± 0.0118
(c)	0.7791 ± 0.0079	-1.1055 ± 0.0057	-0.5893 ± 0.0126	1.0002 ± 0.0091	0.5011 ± 0.0274	-1.7646 ± 0.0199

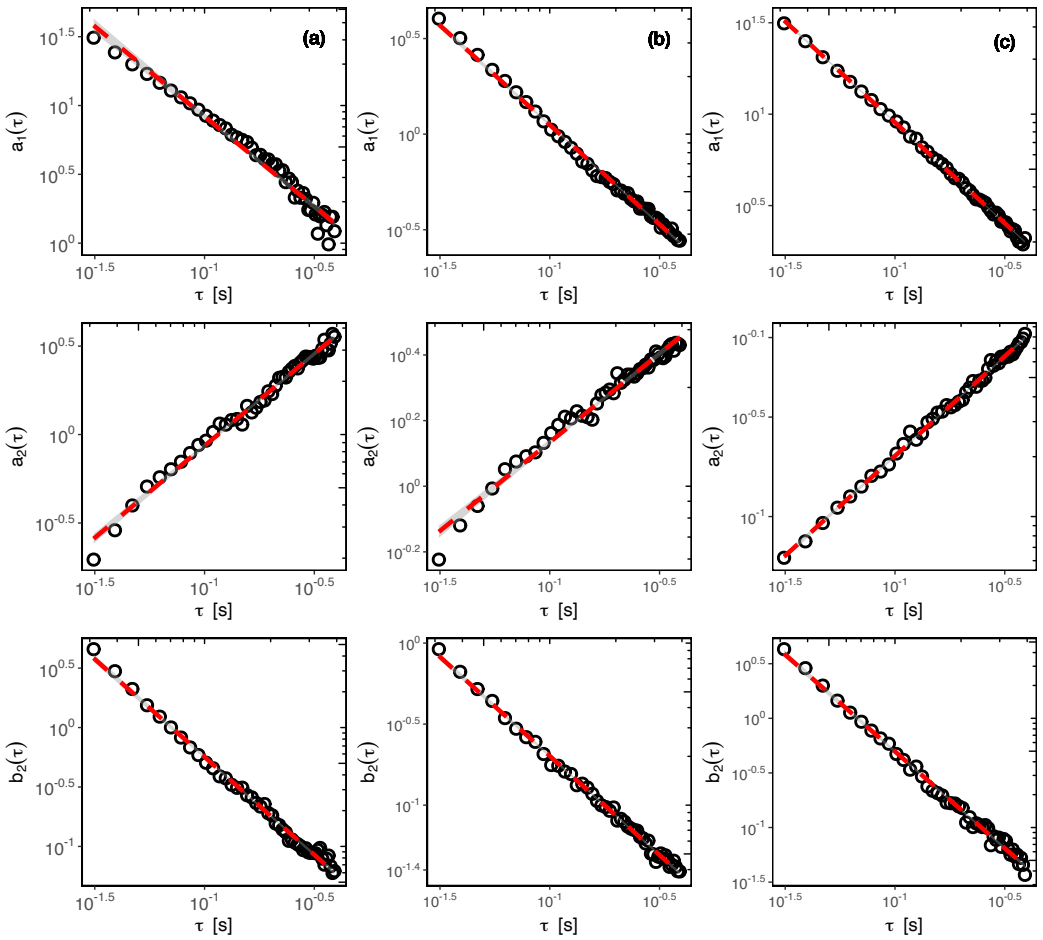

Figure 5: Linear dependence of the parameters a_1, a_2, b_2 in Eqs. (7) and (8) on the double logarithmic scale: (a) near the bow shock (BS), (b) inside the magnetosheath (SH), and (c) near the magnetopause (MP). The dashed red lines, with the standard error illustrated by gray shade, show the best fits to the calculated parameters.

Stationary Solution

By using the linear and parabolic fits of Figures (4) and (5) the stationary solutions of Equation (5) become the well-known continuous kappa distributions (also known as Pearson type VII distribution), which probability density function (PDF) is defined as [Macek et al.(2023)]:

$$p_s(b,\tau) = \frac{N_o}{\left[1+\frac{1}{\kappa}\left(\frac{b}{b_o}\right)^2\right]^{\kappa}} = \frac{N_o'}{\left[a_2(\tau)+b_2(\tau)b^2\right]^{1+\frac{a_1(\tau)}{2b_2(\tau)}}} \tag{17}$$

with $\kappa = 1 + a_1(\tau)/[2b_2(\tau)]$ and $b_o^2 = a_2(\tau)/b_2(\tau)/\kappa = a_2(\tau)/[b_2(\tau)+a_1(\tau)/2]$ (for $a_2(\tau) \neq 0,\ b_o(\tau) \neq 0$) satisfying the normalization, $\int_{-\infty}^{+\infty} p_s(b,\tau)db = 1$, $N_o = p_s(0,\tau) = \frac{\Gamma(\kappa)}{b_o\sqrt{\pi\kappa}\Gamma(\kappa-1/2)}$ and $N_o' = N_o \cdot [a_2(\tau)]^{\kappa}$, with the boundary condition $p_s(b \to \pm\infty,\ \tau) \to 0$. For $\kappa \to \infty$, the distribution approaches the normal Gaussian distribution $N_o \exp\left(-\frac{b^2}{2\sigma^2}\right)$ with the standard deviation $\sigma = b_o/\sqrt{2}$ and the normalization $N_o = \frac{1}{\sigma\sqrt{2\pi}}$.

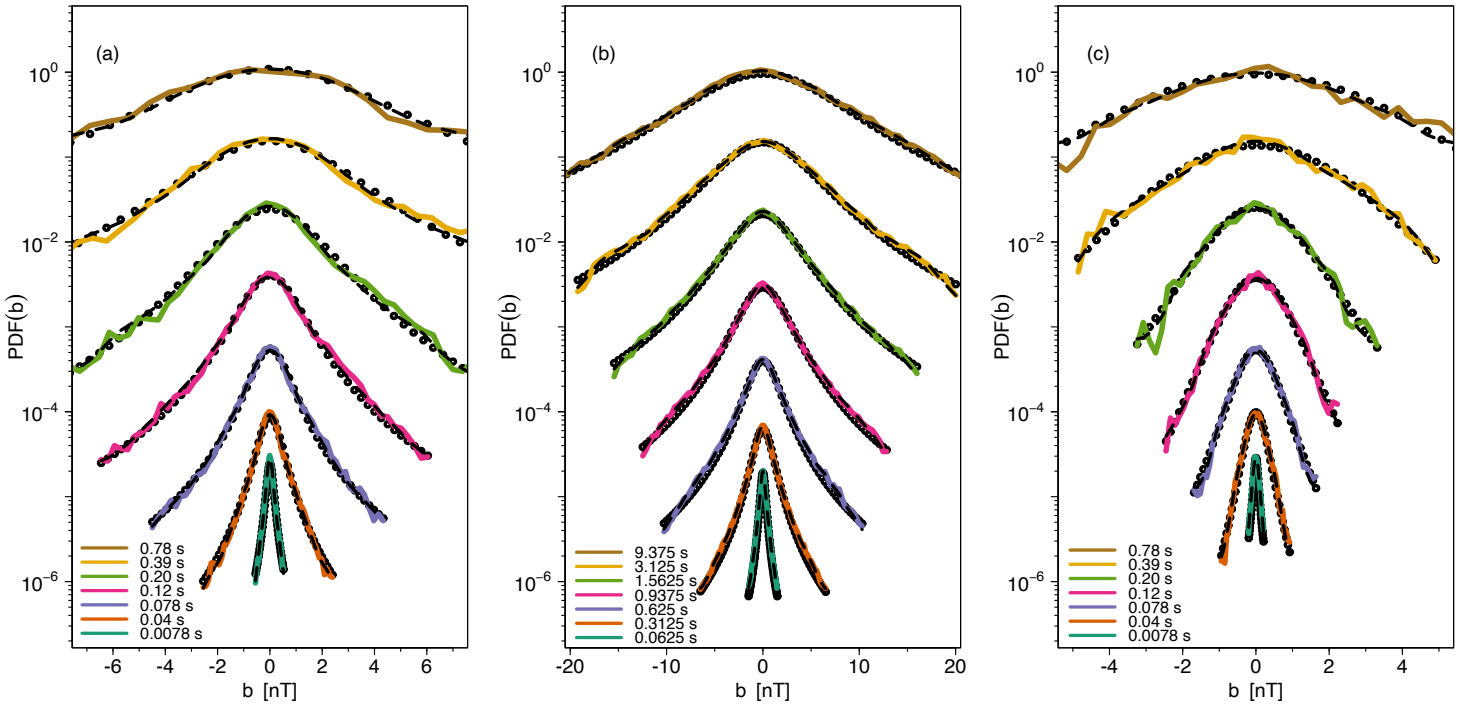

Figure 6: The empirical probability density functions (various continuous colored lines) for a total strength of magnetic field $B = |\mathbf{B}|$, which correspond to cases in Fig. 1compared with the non-stationary (dashed lines) and the stationary (open circles) solutions of the Fokker-Planck equation, for various time-scales (shifted from bottom to top) τ = 0.0078, 0.04, 0.078, 0.12, 0.2, 0.39, and 0.78 s in cases (a) and (c), and τ = 0.0625, 0.3125, 0.625, 0.9375, 1.5625, 3.125, 9.375 s in case (b).

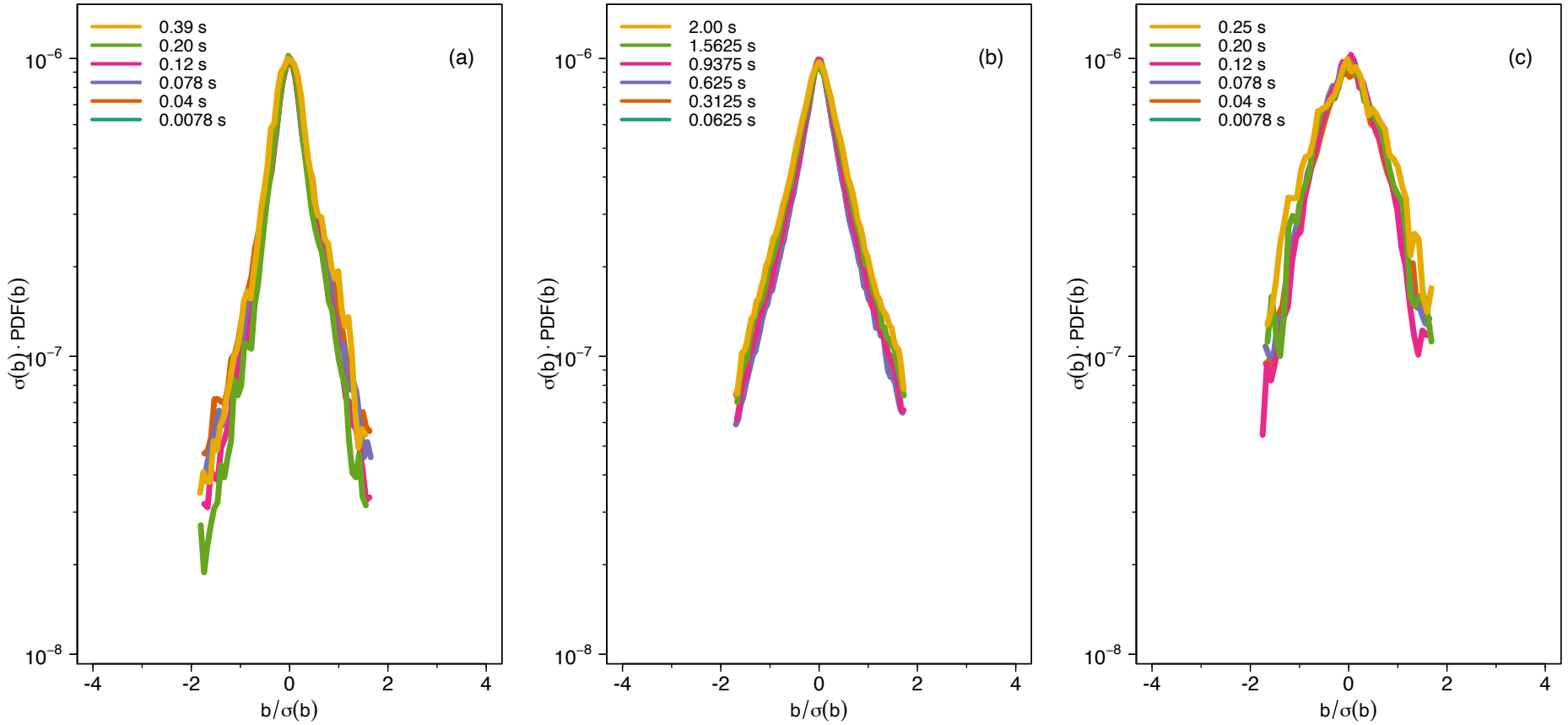

Figure 7: A universal *scale-invariance* of the collapsing probability density functions (PDFs) of b rescaled by the respective standard deviations $\sigma_{b,\tau}$, corresponding to the kappa distributions in Figure 6 on the kinetic scales up to (a) $\tau \sim 0.4$ s, (b) $\tau \sim 2$ s, and (c) $\tau \sim 0.25$ s, correspondingly.

Conclusions

- *Magnetospheric Multiscale* and *Parker Solar Probe* missions with unprecedented high millisecond time resolution of magnetometer data allow us to investigate turbulence on very small kinetic scales [Macek et al.(2023), Macek & Wójcik(2023)]. In this paper we have looked at the *MMS* observations above 20 Hz, where the magnetic spectrum becomes very steep, with the slope, close to -16/3, resulting possibly from interaction between coherent structures [Macek et al.(2018)].

- Following our previous studies in the inertial region [Strumik & Macek(2008a), Strumik & Macek(2008b)] we have shown for the first time that the Chapman-Kolmogorov equation, which is a necessary condition for the Markovian character of turbulence, is satisfied, exhibiting a local transfer mechanism of turbulence cascade also on much smaller kinetic scales. Moreover, we have verified that in this case the Fokker-Planck equation is reduced to drift and diffusion terms at least for scales smaller than (a) $\tau \sim 0.8$ s, (b) $\tau \sim 9$ s, and (c) $\tau \sim 0.8$ s, correspondingly.

- In particular, similarly as for *Parker Solar Probe* (*PSP*) data analyzed by [Benella et al.(2022)] these lowest-order coefficients are linear and quadratic functions of magnetic field, which correspond to the generalized Ornstein--Uhlenbeck processes. We have also recovered a similar universal *scale--invariance* of the probability density functions (PDFs) up to kinetic scales of (a) $\tau \sim 0.4$ s, (b) $\tau \sim 2$ s, and (c) $\tau \sim 0.25$ s, correspondingly.

- It is interesting to note that for moderate scales we have also non-Gaussian kappa distribution, which for the smallest values of the available scale of 7.8 ms, is approximately described by a very peaked shape close to the Dirac delta function. We also show that the normal Gaussian distribution is recovered for timescales two orders larger (with a large value of kappa parameter).

- We hope that our observation of Markovian futures in solar wind turbulence will be important for understanding the relationship between deterministic and stochastic properties of turbulence cascade at kinetic scales in complex astrophysical systems.

Acknowledgments. **W**e thank Marek Strumik for discussion on the theory of Markov processes. We are grateful for the efforts of the entire *MMS* mission, with J. L. Burch, Principle Investigator, C. T. Russell and the magnetometer team, including development, science operations, and the Science Data Center at the University of Colorado. The magnetic field data from the magnetometer are available online from `http://cdaweb.gsfc.nasa.gov`. We acknowledge B. L. Giles, Project Scientist, for information about the magnetic field instrument, D. G. Sibeck and M. V. D. Silveira for discussions during previous visits by W. M. M to the NASA Goddard Space Flight Center. The data have been processed by D. Wójcik using the statistical programming language R.

This work has been supported by the National Science Centre, Poland (NCN), through grant No. 2021/41/B/ST10/00823.

Collaboration

W. M. Macek[1,2,3], M. V. D. Silveira[1,4], D. G. Sibeck[1], B. L. Giles[1], and J. L. Burch[5]

[1] NASA Goddard Space Flight Center, Code 6740, Greenbelt, MD 20771, USA

[2] Institute of Physical Sciences, Faculty of Mathematics and Natural Sciences,

Cardinal Stefan Wyszyński University, Wóycickiego 1/3, 01-938 Warsaw, Poland;

[3] Space Research Centre, Polish Academy of Sciences, Bartycka 18 A, 00-716 Warsaw, Poland;

[4] Catholic University of America, Washington, DC 20064, USA

[5] Southwest Research Institute, San Antonio, TX, USA

e-mail: macek@cbk.waw.pl, `http://www.cbk.waw.pl/~macek`

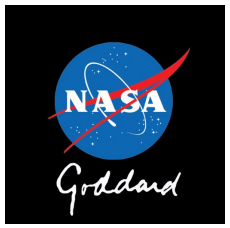

References

[Benella et al.(2022)] Benella, S., Stumpo, M., Consolini, G., et al. 2022, Markovian features of the solar wind at subproton scales, Astrophysical Journal Letters, 928, L21, https://doi.org/10.3847/2041-8213/ac6107.

[Biskamp(2003)] Biskamp, D. 2003, Magnetohydrodynamic Turbulence (Cambridge, UK: Cambridge University Press).

[Bruno & Carbone(2016)] Bruno, R., & Carbone, V. 2016, Lecture Notes in Physics, Vol. 928, Turbulence in the Solar Wind (Springer International Publishing, Berlin).

[Chang(2015)] Chang, T. T. S. 2015, An Introduction to Space Plasma Complexity (Cambridge: Cambridge University Press).

[Frisch(1995)] Frisch, U. 1995, Turbulence. The legacy of A.N. Kolmogorov (Cambridge: Cambridge University Press).

[Macek et al.(2018)] Macek, W. M., Krasińska, A., Silveira, M. V. D., Sibeck, D. G., Wawrzaszek, A., Burch, J. L., & Russell, C. T. 2018, Magnetospheric Multiscale observations of turbulence in the magnetosheath on kinetic scales, *Astrophysical Journal Letters*, 864, L29, https://doi.org/10.3847/2041-8213/aad9a8.

[Macek et al.(2023)] Macek, W. M., Wójcik, D. & Burch, J. L. 2023, *Magnetospheric Multiscale* observations of Markov turbulence on kinetic scales, arXiv=2211.05098, *Astrophysical Journal*, 943, 152, https://doi.org/10.3847/1538-4357/aca0a0.

[Macek & Wójcik(2023)] Macek, W. M., & Wójcik, D. 2023, Statistical analysis of stochastic magnetic fluctuations in space plasma based on the MMS mission, arXiv=2309.06585, *Monthly Notices of the Royal Astronomical Society*, 526, 5779–5790, https://doi.org/10.1093/mnras/stad2584.

[Rinn et al.(2016)] Rinn, P., Lind, P., Wächter, M., & Peinke, J. 2016, The Langevin approach: An R Package for modeling Markov processes, *Journal of Open Research Software*, 4, e34, https://doi.org/10.5334/jors.123.

[Risken (1996)] Risken, H. 1996, The Fokker-Planck Equation: Methods of Solution and Applications, Springer Series in Synergetics (Springer Berlin Heidelberg).

[Strumik & Macek(2008a)] Strumik, M., & Macek, W. M. 2008a, Testing for Markovian character and modeling of intermittency in solar wind turbulence *Physical Review E*, 78, 026414, https://doi.org/10.1103/PhysRevE.78.026414.

[Strumik & Macek(2008b)] Strumik, M., & Macek, W. M. 2008b, Statistical analysis of transfer of fluctuations in solar wind turbulence, *Nonlinear Processes in Geophysics*, 15, 607–613, https://doi.org/10.5194/npg-15-607-2008.